# Quantifying movements of corrosion products in reinforced concrete using x-ray attenuation measurements

**Pease, Bradley Justin; Michel, Alexander; Stang, Henrik**

*Published in:*
Proceedings of the 2nd International Conference on Microstructure Related Durability of Cementitious Composites

*Publication date:*
2011

*Document Version*
Publisher's PDF, also known as Version of record

Pease B, Michel A, Stang H, "Quantifying movements of corrosion products in reinforced concrete using x-ray attenuation measurements," 2nd Int. Conf. on Microstructure Related Durability of Cementitious Composites (MicroDurability), Amsterdam, The Netherlands, 11-13 April, 2012

# QUANTIFYING MOVEMENTS OF CORROSION PRODUCTS IN REINFORCED CONCRETE USING X-RAY ATTENUATION MEASUREMENTS

**Brad J. Pease (1), Alexander Michel (1) and Henrik Stang (1)**

(1) Technical University of Denmark, Department of Civil Engineering, Kgs. Lyngby, Denmark

## Abstract

Corrosion of steel reinforcement, embedded in concrete, may substantially degrade concrete structures due to the expansive nature of corrosion products. Expansion of corrosion products cause tensile stresses to develop and cracks to form in concrete. Extensive research has focused on corrosion-induced damage of concrete, typically by monitoring and quantifying the formation of cracks in concrete surrounding corroding reinforcement. Based on the type of experimental data numerous corrosion-induced damage models have been developed. One common conclusion from these models is that a certain amount of corrosion products move into the concrete without generating tensile stresses and cracks in the concrete. Typically, corrosion products are thought to occupy pores, interfacial defects, and/or air voids located near the concrete-steel interface and stresses develop only after filling of these pores. Further, the amount of corrosion products the concrete can accommodate is directly related to model predictions of time-to-cracking. While some have attempted to measure the size of the region where corrosion products are accommodated using destructive and invasive approaches, additional techniques are needed to more accurately assess this vital parameter.

This paper describes the use of x-ray attenuation measurements to monitor and quantify the movements of reinforcement corrosion products into mortar surrounding corroding reinforcement. Corrosion is induced by application of direct current to the embedded reinforcement. X-ray attenuation measurements are also capable of detecting cracks. Therefore, this approach provides a direct measurement of the amount and location of reinforcement corrosion products required to induce cracking. Results of a parametric investigation on the impact of water-to-cement ratio (0.30, 0.40, and 0.50) and corrosion rate are presented. Results from this non-destructive experimental approach should provide further insights for the modelling of reinforcement corrosion and corrosion-induced damage of concrete structures.

## 1. INTRODUCTION

Corrosion-induced deterioration of reinforced concrete structures is a costly problem, which has been the focus of numerous research projects resulting in the development of models to describe the corrosion-induced cracking process. Comparisons of empirical [1], analytical [2,3], and numerical [4-6] model results to experimentally observed time to corrosion-induced cracking have indicated that the concrete immediately surrounding a corroding rebar can accommodate some amount of corrosion products without the development of tensile stresses. This region of concrete, referred to as the corrosion accommodating region (CAR), results in a prolonged time to corrosion-induced cracking. The terms "porous" or "diffusion" zone commonly used to describe this region, which the authors feel are misleading terms, are intentionally avoided here (see [7] for additional discussion). Nevertheless, experimental methods for observing the size of the CAR are limited and values, which range from 0.002-0.12 mm in the literature [3], are typically determined as a fitting parameter to adjust model outputs to experimental results.

This paper presents a parametric investigation on the impact of water-to-cement ratio (w/c) and corrosion current density, i.e. corrosion rate, on corrosion-induced cracking behaviour using the x-ray attenuation measurement technique. X-ray attenuation measurements, which assess the amount and location of corrosion products and the time of corrosion-induced cracking, provide a direct measure of the size of the CAR [7].

## 2. EXPERIMENTAL APPROACH

### 2.1 Materials and specimen preparation

Experiments were conducted on reinforced mortar specimen of varying water-to-cement ratios (w/c), including 0.30, 0.40 and 0.50, using Aalborg Rapid® portland cement (Type 52.5N cement [8]). Mixtures contained 375 kg/m$^3$ cement and 50% by volume fine aggregates (0–4 mm Class E sand in accordance with [9]). No chlorides were added to the mix, as corrosion was induced by applying electrical current as described below. Superplasticizer (Sika ViscoCrete 2300-HE®) was used for 0.30 and 0.40 w/c mixtures at dosages of 0.50% and 0.30% of cement content, respectively, to maintain similar workability to the 0.50 w/c mixture. A smooth 10 mm steel dowel rod was embedded in the centre of the 10×10×50 cm$^3$ prism as illustrated in Fig. 1. The mortars were mixed using a standard mortar mixer and mixing procedures [10], placed in forms and consolidated by rodding and vibrating.

After casting, mortar prisms were stored in moulds for 24 hours under a plastic sheet in laboratory conditions (i.e., 20±2°C) and then demoulded. Upon demoulding, the specimens were stored under water for additional 6 days at 20 ±2°C. The 50 cm long prisms were cut perpendicular to the embedded steel bar in 2.3 cm lengths using a water-cooled concrete saw, resulting in 10×10×2.3 cm$^3$ samples (see Fig. 1). A lead wire was soldered to the reinforcement to allow for accelerated corrosion. A DC regulator was used to impress an electrical current through a ruthenium/iridium mixed metal oxide activated titanium mesh counter electrode. Tap water (no chlorides added) provided an electrical connection between the working (steel bar) and counter electrodes by partially submerging specimens in individual acrylic ponds. The water level was maintained at approximately 1 cm below the steel bar and ponds were refilled daily. Three current densities were used for each w/c investigated (9 specimens in total), including 10, 50, and 100 μA/cm$^2$ or approximately 0.12, 0.58, and 1.16 mm/year according to Faraday's law (assuming the formation of $Fe^{2+}$).

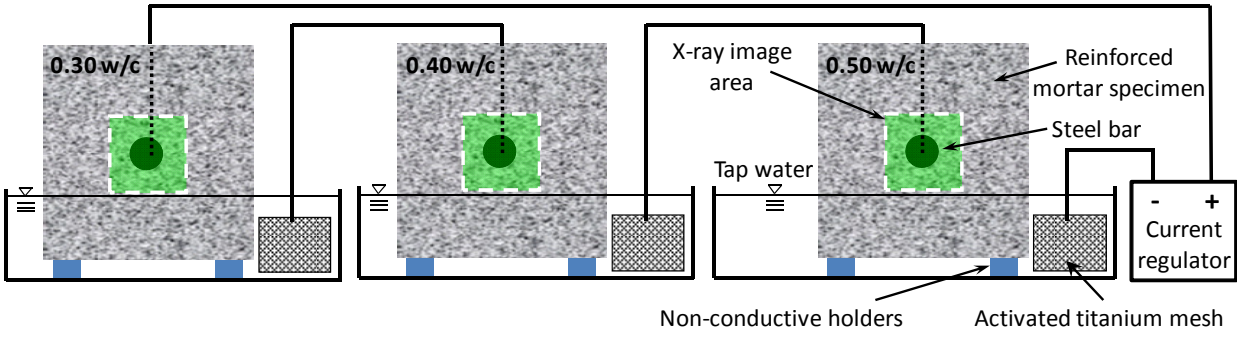

Figure 1: Experimental set up for accelerated corrosion applying an impressed current with x-ray measurement area indicated

### 2.2 X-ray attenuation measurement technique

A GNI x-ray facility located at the Technical University of Denmark [11] was used for x-ray attenuation measurements. Fig. 2 shows the x-ray source (a polychromatic x-ray source), a 252×256 pixel x-ray camera, and a programmable three-axis motion frame for moving the source and camera, which are housed in a shielded, environmentally controlled chamber. The x-ray source excitation settings used were a voltage of 80 keV and a current of 75 μA. The x-ray source was automatically ramped up to these settings over a 120 second "warmup" period and the x-ray source was allowed to stabilize for 60 seconds prior to recording images. A single measurement consisted of 60 x-ray camera images recorded with an integration time of 1 second each (i.e., 60 second integration time). The intensities measured by individual pixels from the 60 images were summed. So-called dark current images (i.e., x-ray camera images recorded while x-ray source is turned off), recorded prior to all x-ray measurements, were subtracted from the measured intensities.

The composite system shown in Fig. 2(b) can be used to derive an equation that relates the reduction in number of x-ray photons passing through a non-corroded specimen, $I_{non}$ and a specimen with corrosion products, $I_{corr}$ to the change in concentration of corrosion products, $\Delta c_{cp}$ (g/cm$^3$) [7]:

$$\Delta c_{cp} = -\frac{\rho_{cp}}{\mu_{ef,cp} \cdot t} \cdot ln\left(\frac{I_{corr}}{I_{non}}\right) \quad (1)$$

where $\rho_{cp}$ is the density of the corrosion product (g/cm$^3$), $\mu_{ef,cp}$ is the effective attenuation coefficient of corrosion product (i.e., the attenuation coefficient of corrosion product as measured through the 23 mm specimens, cm$^{-1}$), and $t$ is the specimen thickness (cm). The assumed corrosion product is $Fe_2O_3$ (assumption confirmed previously in [7]), which has a density of 5.24 g/cm$^3$ and a measured effective attenuation coefficient of 2.14 cm$^{-1}$. Prior to application of corrosion current, a total of 3 measurements of $I_{non}$ were taken (i.e., 180 total images). During accelerated corrosion testing, measurements were recorded every 4, 12 and 24 hours for the 100, 50, and 10 μA/cm$^2$ specimens, respectively, until cracks were clearly visible in calculated (Eq. 1) images. Additional information on the application of the x-ray measurement technique to monitor reinforcement corrosion is available in the literature [7,12].

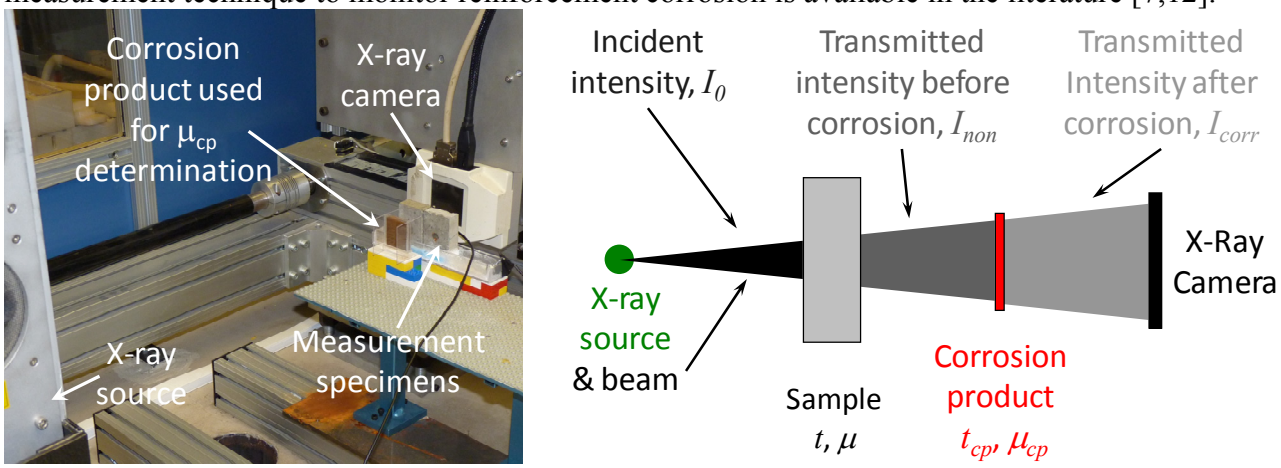


(a) (b)

Figure 2: (a) X-ray attenuation measurement system with experimental setup consisting of the x-ray source and camera along with the specimen, and (b) effect of change in concentration of corrosion products on x-ray attenuation measurements as described by a composite of the initial specimen and a thickness of corrosion products representing reinforcement corrosion.

## 3. RESULTS

### 3.1 X-ray image analysis

Fig. 3 shows typical calculated x-ray images using Eq. 1, and identifies the key features of the specimens and measurements. All images consist of 64,512 measurement points (252x256 pixels) with a corresponding physical area of approximately 3,136 $\mu m^2$ (56 x 56 $\mu m^2$) per pixel. Image details include the 10 mm diameter smooth rebar which appears in black, corrosion products indicated by a light grey to white colour, cracks (Figs. 3(b) and (c)) appear as dark grey to black, and the wire used to induce corrosion. The 2.3 cm thick rebar effectively attenuates all x-ray photons, resulting in values approaching negative infinity. Corrosion products form around the rebar and penetrate into the surrounding mortar in a non-uniform manner (discussed in detail below). Cracks eventually form in the mortar, as clearly seen in Figs. 3(c) and, to a lesser degree, (b). Cracks can be difficult to see initially in calculated images, suggesting time to cracking could be more accurately assessed using a different approach (e.g., photogrammetry, passive acoustic emission, etc.). The wire, which is a source of 'noise' in the data, extends from the right side of the rebar in Fig. 3(c) and continues out of the measured area. The wire appears in various shades of grey, yielding false indications of either corrosion products or cracks, due to small movements of the wire. As shown in Fig. 4(a), the wire region was removed prior to all following analyses.

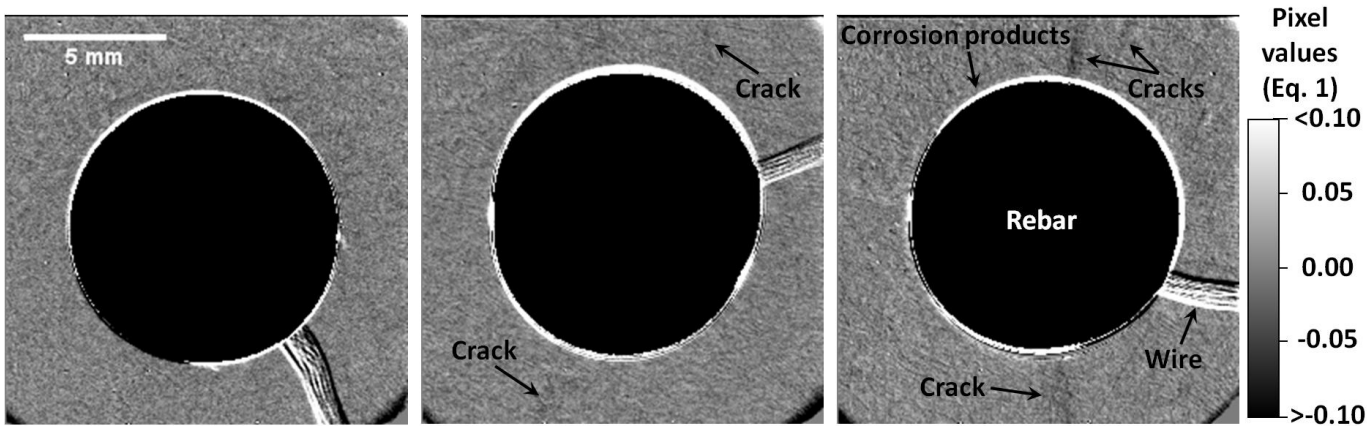


(a) (b) (c)

Figure 3: Calculated x-ray images (Eq. 1) after 7.3 days of corrosion at 1.16 mm/year (100 $\mu A/cm^2$) for (a) 0.30, (b) 0.40, and (c) 0.50 w/c mortar specimens with scale indicating the corresponding calculated values.

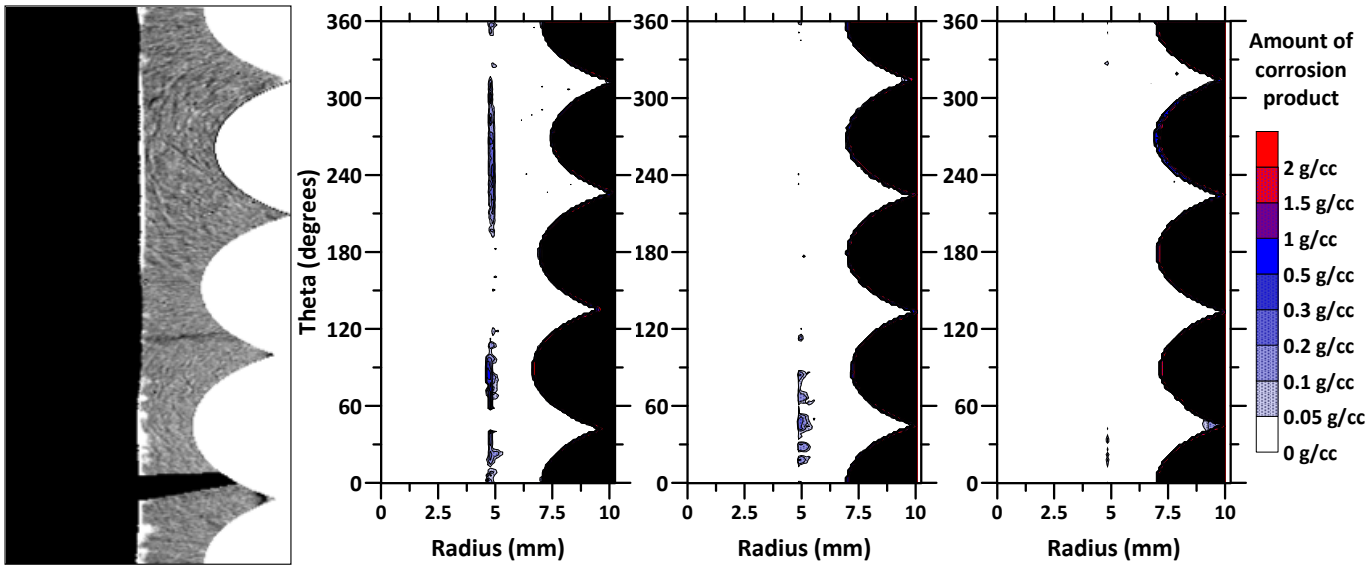


(a) (b) (c) (d)

Figure 4: Polar transformations (a) of calculated x-ray image (Eq. 1) and resulting contour plots of corrosion product concentrations in 0.30 w/c specimens after 74 days of corrosion at (a,b) 1.16 mm/year (100 μA/cm$^2$), (c) 0.58 mm/year (50 μA/cm$^2$), and (d) 0.12 mm/year (10 μA/cm$^2$). Scale from Fig. 3 applies to (a) polar transformation of calculated x-ray image.

Fig. 4 illustrates results of an additional image analysis approach, i.e. polar transformation of calculated images. Polar transformation and the resulting contour plots in Figs. 4(b-d) provide location-dependent information on the concentration of corrosion products as a function of distance from the rebar surface. Results presented below were extracted from polar transformation images by summing the total concentration of corrosion products at various radii from the rebar surface.

### 3.2 Impact of water-to-cement ratio

Fig. 3 provides a qualitative overview on the impact of w/c. Under a constant corrosion rate (1.16 mm/year – 100 μA/cm$^2$) and at a given time (7.3 days) corrosion products appear to penetrate further into mortar as w/c increases. Additionally, the time of observed cracking is delayed with decreased w/c. Fig 3(c) clearly shows multiple cracks in the 0.50 w/c specimen, while cracks are only faintly observed in the 0.4 w/c specimen (Fig. 3(b)) and cracks are not observed in the 0.3 w/c specimen. Cracks were initially observed after 4.2, 5.8, and 9.5 days for 0.50, 0.40, and 0.30 w/c specimens, respectively with a 1.16 mm/year corrosion rate (see Fig. 7(b)). Average tensile strength of three splitting tensile specimen (100 mm diameter, 200 mm high cylinders under identical curing) were 4.5, 5.2, and 6.5 MPa for the 0.50, 0.40, and 0.30 w/c mortars, respectively.

Fig. 5; which presents total concentration profiles of corrosion products at various times, extracted from polar transformation images; provides quantitative information on the impact of w/c. Results indicate higher w/c mortar tends to allow corrosion products to penetrate in greater concentrations at a given time. For example, results from the 1.16 mm/year corrosion rate (Fig. 5(a)) after 1.2 days show concentrations of corrosion products in the 0.50 w/c specimen tend to be higher than the 0.30 w/c specimen. Increased concentrations of corrosion products are also seen at the time of observed cracking for the 0.50 w/c specimen over the 0.30 w/c (except immediately at the rebar surface) even though the 0.30 w/c specimen required an additional 5.3 days of corrosion to crack. Only in the case of the 0.58 mm/year (50 μA/cm$^2$) corrosion rate specimens (Fig. 5(b)) can a higher concentration of corrosion products be observed in the 0.30 w/c specimen after comparable corrosion times. Also, at the time of observed cracking, which occurred after 80 days for the 0.30 w/c specimen compared to 11.5 days for 0.50 w/c, an increased concentration of corrosion products is seen. Fig. 5(c) also clearly illustrates the increase in concentration of corrosion products at a given time for higher w/c.

Fig. 6(a) presents the size of the CAR at the time of observed cracking as a function of w/c (0.12 mm/year corrosion rate specimen remain crack-free, results are presented for the last observation time). The boundary of the CAR was defined as the location with a total radial concentration of corrosion products less than 0.02 g/cm and a gradient of total concentration less than 0.01 g/cm. Results indicate a

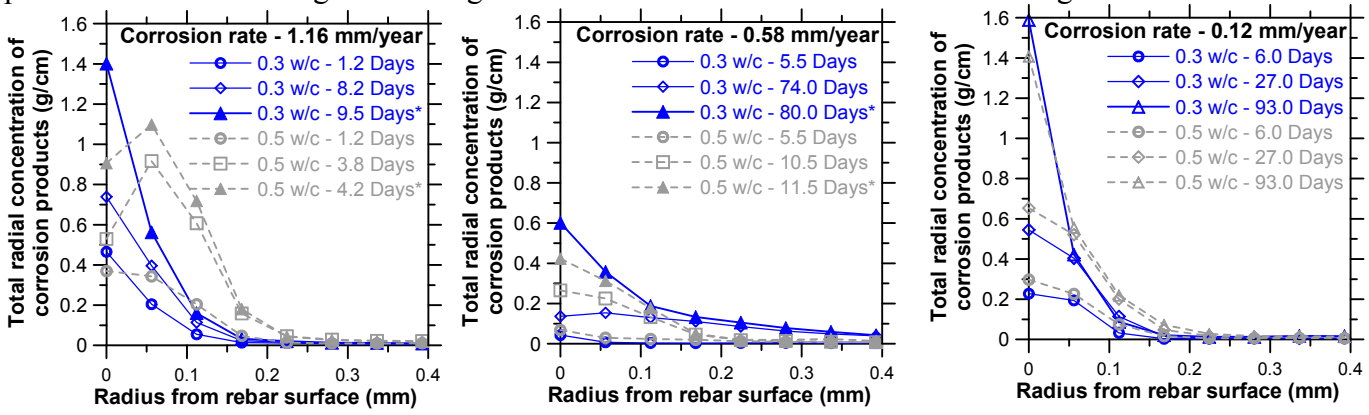


(a) (b) (c)

Figure 5: Profiles of total concentration of corrosion products as a function of radius from the rebar surface at varying times for (a) 1.16 mm/year (100 μA/cm$^2$), (b) 0.58 mm/year (50 μA/cm$^2$), and (c) 0.12 mm/year (10 μA/cm$^2$) (*Indicates total concentration profile at the time of observed cracking).

minimum size of the CAR of approximately 0.17 mm; however, no clear trend on the impact of w/c can be seen. Fig. 6(c) shows the impact of w/c on the total amount of corrosion products detected at the time of cracking. At the 1.16 mm/year corrosion rate, w/c appears to have little impact on the measured amount of corrosion product. However, with reduced corrosion rate, w/c appears to provide for additional amounts of corrosion products. This may indicate the influence of tensile strength is increased for the 0.56 mm/year corrosion rate.

### 3.3 Impact of corrosion rate

Fig. 4 illustrates the general effect of corrosion rate on the location-dependent concentration of corrosion products. As anticipated, at a given time of accelerated corrosion (74 days) less corrosion products are detected in calculated images as corrosion rates decrease. Fig. 5 illustrates the impact of corrosion rate on the total concentration profiles of corrosion products. Fig. 5(b) indicates significantly lower concentrations of corrosion products (near the rebar surface) result in cracking for the 0.58 mm/year (50 μA/cm$^2$) specimens compared to the other corrosion rates investigate. One possible cause for this is discussed in the visual observations section below. However, these results indicate the complexity of the corrosion- induced cracking problem, which involves the tensile strength, stress relaxation, and creep of the mortar, penetration and elastic properties of the corrosion products, among others. Fig. 7 compares the total mass of corrosion products as determined by Faraday's law and by integrating all corrosion products detected in calculated x-ray images for the 0.50 w/c specimens. The figure clearly shows the impact of corrosion rate on the development of corrosion products, and indicates good agreement between x-ray measurements and the theoretical amounts of corrosion products. Fig. 6(a) illustrates that, similarly to w/c, no clear trends on the impact of corrosion rate on the size of the CAR can

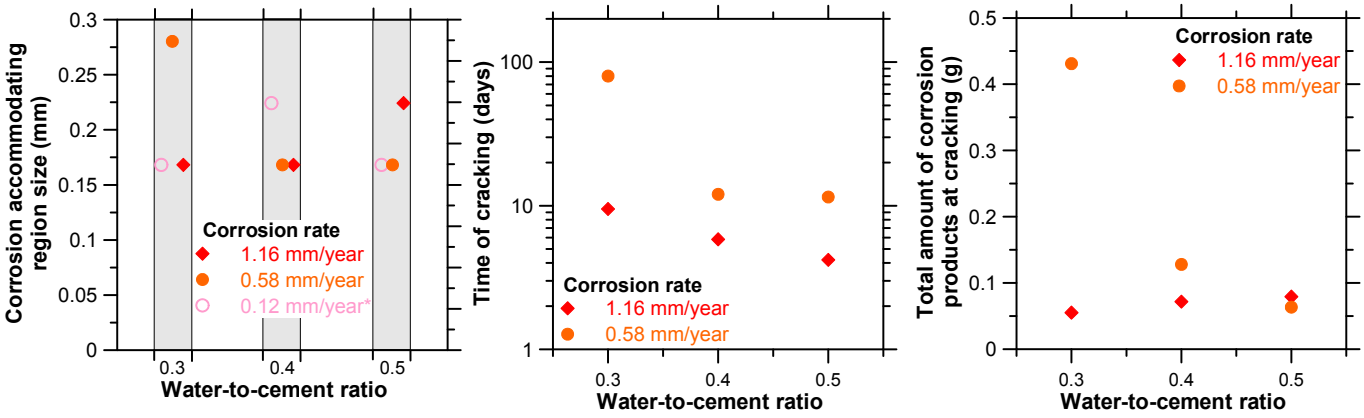


Figure 6: Impact of w/c on (a) size of the corrosion accommodating region at the time of cracking, (b) time of cracking, and (c) total amount of corrosion products detected by x-ray at time of cracking (*Data presented from 93 day measurements for 0.12 mm/year (10 μA/cm$^2$) specimens, cracks have yet to form).

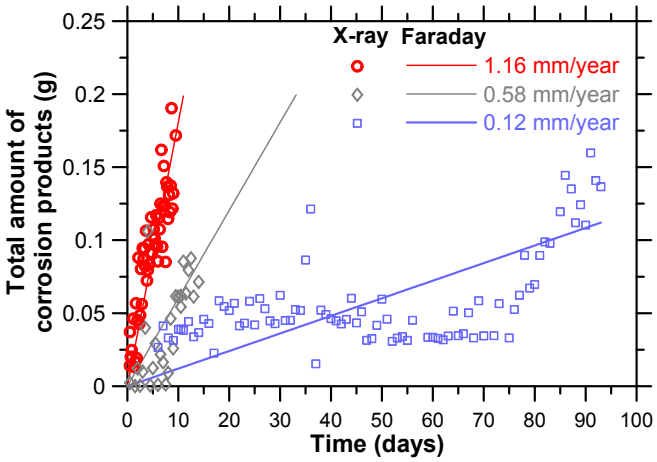


Figure 7: Comparison of total amount of corrosion products obtained by Faraday's law (lines) and x-ray attenuation technique (symbols) at varying corrosion rates, x-ray results from 0.50 w/c specimens.

be ascertained. On the other hand, Fig 6(b) shows reducing the corrosion rate can – as expected – drastically increase the time required to induce cracking.

### 3.4 Visual observations

Figs. 8 and 9 provide visual microscopy images from the 1.16 mm/year (100 μA/cm$^2$) corrosion rate specimens after termination of accelerated corrosion testing at 75 days. The specimens were split to create a new fracture surface (i.e., not the corrosion-induced fracture surface) and the rebar was removed, providing a view of the mortar directly at the steel-mortar interface. As shown in Fig. 8, the appearance of the mortar surface at the interface varies with w/c. In the 0.30 w/c specimen (Fig. 8(a)) some small deposits of corrosion product and rust-staining are seen, while the 0.40 and 0.50 w/c specimens have increasing amounts of the interface surface covered with a significant amount of corrosion products. Fig. 9 shows corrosion products clearly penetrate the 0.40 and 0.50 w/c specimens while comparatively little corrosion product is seen in the new fracture surface of the 0.30 w/c specimen. Visual assessment of the rebar removed from the 0.30 w/c specimen indicated the majority of corrosion products adhered to the rebar, rather than the mortar. Comparison of Figs. 8 and 9 and considering results of calculated x-ray images provides a possible explanation. Fig. 5(a) indicated corrosion products penetrated a similar distance but in higher concentrations in the 1.16 mm/year (100 μA/cm$^2$) corrosion rate specimens with higher w/c, which likely improved the adhesion of the corrosion products to the mortar surface. Similar observations were made for the 0.58 mm/year corrosion rate specimens.

Additional features are identified in the images, including entrapped voids filled with corrosion product (indicated by 'B' and 'C' in Fig 9(b)). The smaller void (shown in the enlarged region) appears to have minute cracks, filled with corrosion product, extending from it.

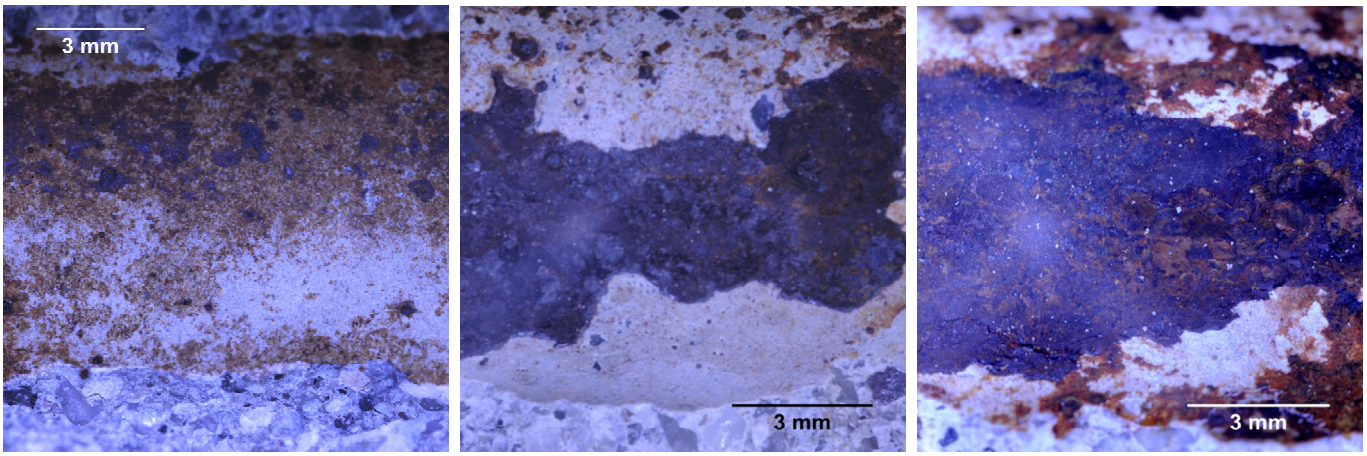


(a) (b) (c)

Figure 8: Images of corrosion products deposited on the mortar at the steel/mortar interface for 1.16 mm/year (100 μA/cm$^2$) specimens with w/c of (a) 0.30, (b) 0.40, and (c) 0.50 (Note: blue colouration caused by light source).

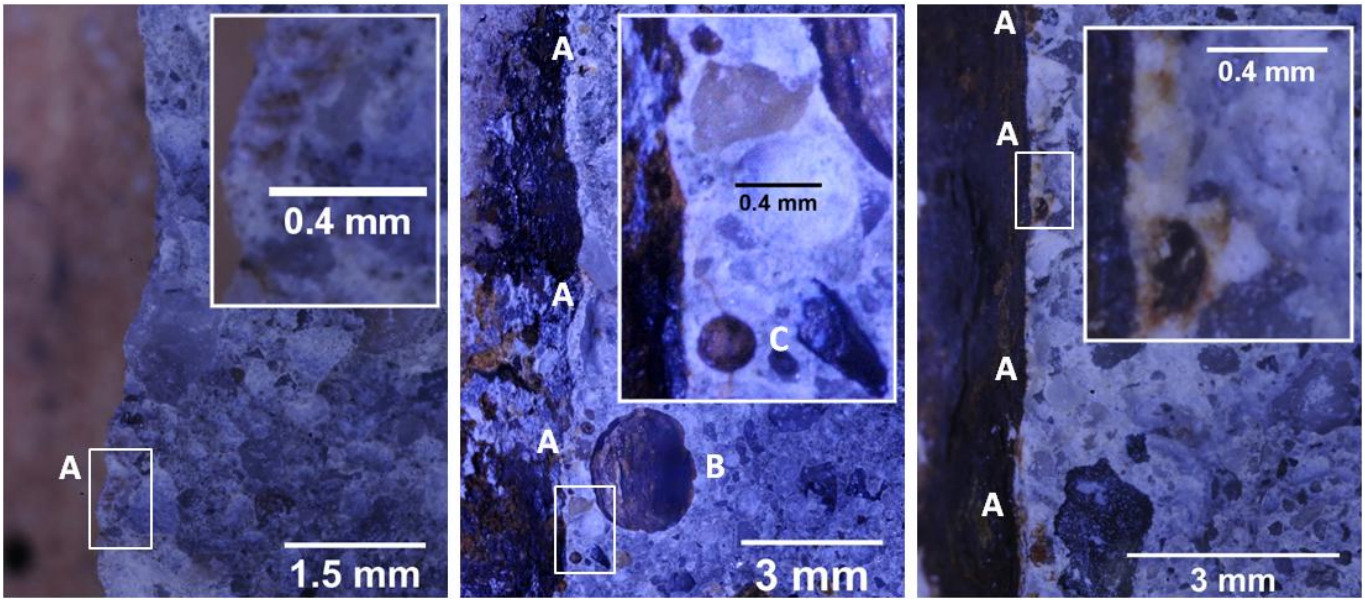


(a) (b) (c)

Figure 9: Images of corrosion products penetrating into mortar from the steel/mortar interface for 1.16 mm/year (100 μA/cm$^2$) specimens with w/c of (a) 0.30, (b) 0.40, and (c) 0.50, and with the following details highlighted: [A]–corrosion products observed, [B]–large entrapped void filled with corrosion products, [C]–small entrapped void filled with corrosion products with cracks extending, [White boxes]–locations of enlarged regions (Note: blue colouration caused by light source).

## 4. DISCUSSION

Results from calculated x-ray images presented in Fig. 5 provide insight into the process by which corrosion products penetrate into mortar. The corrosion products tend to penetrate to a maximum distance from the rebar relatively early in the accelerated corrosion testing, and later the concentration of corrosion products increase closer to the rebar. For example, Fig. 5(a) shows corrosion product concentration profiles for the 0.50 w/c, 1.16 mm/year corrosion rate specimen at various times (1.2, 3.8, and 4.2 days). During early stages, between 1.2 and 3.8 days, corrosion products penetrate to a greater distance from the rebar surface. However, between 3.8 days and 4.2 days (the time of observed cracking), additional corrosion products do not penetrate to such distances from the rebar surface, but concentrations increase near the rebar. This tendency clearly repeats for the 0.30 w/c specimen at the same corrosion rate (Fig. 5(a)) and for the 0.12 mm/year (10 μA/cm$^2$) specimens (Fig. 5(c)). These results indicate that the corrosion products formed early during accelerated corrosion testing effectively obstruct the paths of subsequent corrosion products, leading to the development of tensile stresses and eventual cracking.

Experimental observations of the CAR at time of cracking vary from 0.17-0.28 mm and no clear trends as a function of w/c, corrosion rate (Fig. 6(a)), or time of observed cracking (Fig. 6(b)) can be ascertained. X-ray results presented in Figs. 3 and 4 and visual observations in Fig. 9 indicate the penetration of corrosion products into mortar is highly non-uniform. Local anomalies (e.g., voids, etc.) provide pathways for corrosion products to potentially penetrate far from the rebar surface. In contrast, typical modelling approaches [1-6] assume a uniform corrosion behaviour results in uniform pressure being applied to the surrounding concrete (or mortar) and a single value for the size of the CAR. Therefore, to advance modelling approaches and improve model estimates, the impact of concrete defects near the rebar surface and the implications of a non-uniform corrosion must be considered.

## 5. SUMMARY AND CONCLUSIONS

X-ray attenuation measurements were used to directly measure the amount and location of penetrating corrosion products in reinforced mortar specimens with water-to-cement ratios of 0.30, 0.40, and 0.50 during accelerated corrosion testing. Three corrosion rates were investigated including 1.16, 0.58, and 0.12 mm/year, or 100, 50, and 10 $\mu A/cm^2$, respectively. From the results presented, it can be concluded that:

- Increasing the corrosion rate and/or water-to-cement ratio reduces the time of observed cracking. However, cracks can be difficult to observe in calculated x-ray images, suggesting time to cracking should be assessed using an additional approach.
- Under the investigated conditions, corrosion products typically penetrate to a maximum distance from the rebar relatively early during accelerated corrosion. Subsequently, the concentration of corrosion products increases closer to the rebar. It is hypothesized that corrosion products formed early in accelerated corrosion testing obstruct the penetration of subsequent corrosion products. Once the concentration of corrosion products reaches a critical level tensile stresses develop and the mortar cover eventual cracks.
- The penetration of corrosion products into mortar is highly non-uniform and is effected by local defects, such as entrapped voids or interfacial defects. Advanced modelling approaches should likely consider the impact of concrete defects near the rebar surface and implications of non-uniform corrosion to more accurately represent reality.

## ACKNOWLEDGEMENTS

Financial contributions from the Danish Expert Centre for Infrastructure Constructions and the project 'Sustainable Rehabilitation of Civil and Building Structures' funded by Nordic Innovation Centre, project no. 08190 SR are greatly appreciated. The second author gratefully acknowledges the financial support of Femern Bælt A/S, Sund & Bælt Holding A/S, and The Danish Agency for Science, Technology and Innovation.

## REFERENCES

[1] Alonso, C., Andrade, C., Rodriguez, J., Diez, J.M., "Factors controlling cracking of concrete affected by reinforcement corrosion," Materials and Structures Vol. 31, pp. 435-441, 1998.
[2] Bažant, Z., "Physical model for steel corrosion in concrete sea structures - application," J. of the Structural Division, Vol. 105, pp. 1155–1166, 1979.
[3] Chernin, L. , Val, D.V., Volokh, K.Y., "Analytical modelling of concrete cover cracking caused by corrosion of reinforcement," Materials and Structures, Vol. 43(4), pp. 543–556, 2010.
[4] Molina, F.J., Alonso, C., Andrade, C., "Cover cracking as a function of rebar corrosion: part 2—numerical model," Materials and Structures, Vol. 26(9), pp. 532–548, 1993.
[5] Liu, Y., Weyers, R., "Modeling the time-to-corrosion cracking in chloride contaminated reinforced concrete," ACI Materials Journal, Vol. 95(6), pp. 675–681, 1998.
[6] El Maaddawy, T., Soudki, K., "A model for prediction of time from corrosion initiation to corrosion cracking," Cement and Concrete Composites, Vol. 29(3), pp. 168–175, 2007.
[7] Michel, A., Pease, B., Geiker, M.R., Stang, H., Olesen, J.F., "Monitoring reinforcement corrosion and corrosion-induced cracking using non-destructive x-ray attenuation measurements," Cement and Concrete Research, Vol. 41(11), pp. 1085-1094, 2011.
[8] DS/EN 197-1 Cement—Part 1: Composition, specification and conformity criteria for common cements, Danish Standards Association, 2001 29 pp.
[9] DS-2426, Concrete—Materials—Rules for application EN 206-1 in Denmark, Danish Standards Association, 2004.
[10] ASTM Standard C305 "Standard Practice for Mechanical Mixing of Hydraulic Cement Pastes and Mortars of Plastic Consistency" ASTM Int., West Conshohocken, PA, 2011, DOI: 10.1520/C0305-11
[11] www.gni.dk GNI X-ray System, Technical University of Denmark, 2010.
[12] Michel, A., Pease, B., Peterova, A., Geiker, M., "Experimental determination of the penetration depth of corrosion products and time to corrosion-induced cracking in reinforced cement based materials," Submitted to Int. Congress on Durability of Concrete, Trondheim, Norway, June 17-21, 2012.